The Astrophysical Journal Letters, 979:L16 (8pp), 2025 January 20 https://doi.org/10.3847/2041-8213/ada611

The Occurrence of Powerful Flares Stronger than X10 Class in Solar Cycles

Baolin Tan[1,2], Yin Zhang[1], Jing Huang[1,2], and Kaifan Ji[3,4]
[1] CAS Key Laboratory of Solar Activity, National Astronomical Observatories of Chinese Academy of Sciences, Datun Road 20A, Chaoyang District, Beijing 100012, People's Republic of China; bltan@nao.cas.cn
[2] School of Astronomy and Space Sciences, University of Chinese Academy of Sciences, Beijing 100049, People's Republic of China
[3] Yunnan Observatories, Chinese Academy of Sciences, P.O. Box 110, Kunming 650011, People's Republic of China
[4] Yunnan Key Laboratory of Solar Physics and Space Science, Kunming 650216, People's Republic of China
Received 2024 June 14; revised 2024 December 31; accepted 2025 January 4; published 2025 January 16

Abstract

Solar flares stronger than X10 (S-flares, >X10) are the highest-class flares that significantly impact on the Sun's evolution and space weather. Based on observations of Geostationary Orbiting Environmental Satellites at soft X-ray wavelength and the daily sunspot numbers (DSNs) since 1975, we obtained some interesting and heuristic conclusions: (1) both S-flares and the more powerful extremely strong flares (ES-flares, >X14.3) mostly occur in the late phases of solar cycles (SCs) and low-latitude regions on the solar disk; (2) similar to X-class flares, the occurrence of S-flares in each SC is somewhat random, but the occurrence of ES-flares seems to be dominated by the mean DSN (V_m) and its rms deviation during the valley phase (V_d) before the cycle: the ES-flare number is strongly correlated with V_d, and the occurrence time of the first ES-flare is anticorrelated with V_d and V_m. These facts indicate that the higher the V_m and V_d, the stronger the SC, the more the ES-flares, and the earlier they occurred. We propose that the Sun may have a low-latitude active zone (LAZ), and most ES-flares are generated from the interaction between the LAZ and the newly emerging active regions. The correlations and the linear regression functions may provide an useful method to predict the occurrence of ES-flares in an upcoming SC, which derives that SC 25 will have about 2 ± 1 ES-flares after the spring of 2027.

Unified Astronomy Thesaurus concepts: Solar cycle (1487); Solar flares (1496)

1. Introduction

Solar eruptions refer to the rapid and violent magnetic energy release in the low atmosphere of the Sun, including solar flares, coronal mass ejections (CMEs), and various plasma jets. Among them, solar flares are the most spectacular events, and CMEs and jets are more or less physically linked to flares (R. A. Harrison 1995). Generally, solar flares are classified into A-, B-, C-, M-, and X-class (T. Bai & P. A. Sturrock 1989), which denotes the order of peak flux of soft X-ray (SXR) emission (F_{sxr}) observed by Geostationary Orbiting Environmental Satellites (GOES) at a wavelength of 1–8 Å on a logarithmic scale: $A = 10^{-8}$, $B = 10^{-7}$, $C = 10^{-6}$, $M = 10^{-5}$, and $X = 10^{-4}$ W m^{-2}, respectively; the subdivided class is added an additional digit, such as M5, which means a solar flare with SXR emission peak flux of 5.0×10^{-5} W m^{-2}. When $F_{sxr} > 10^{-3}$ W m^{-2}, that means the flare is stronger than X10 and can be denoted as an S-flare. Thousands of flares occurred in each solar cycle (SC). For example, SC 23 had 6 S-flares, 167 X-class flares, 1444 M-class flares, and 12,995 C-class flares. Although, according to the definition of superflares (B. E. Schaefer et al. 2000; H. Maehara et al. 2012; T. Shibayama et al. 2013; Y. Notsu et al. 2019), even the strongest solar flares recorded in history (for example, Carrington event on 1859 September 1 with a class of nearly X80; H. Hayakawa et al. 2023) still did not meet the criterion of superflares (A. G. Emslie et al. 2012; E. W. Cliver et al. 2022). However, S-flares are the most powerful eruptions to have occurred in the whole solar system and have the greatest impact on the space environment. This work attempts to identify certain patterns of S-flares from long-term observational data on SXR/GOES and the daily sunspot number (DSN) since 1975, which may be beneficial for predicting solar activity and studying the long-term evolution of the Sun.

Many people predicted that SC 25 should be stronger than SC 24 (Pesnell & Schatten 2018, W. Guo et al. 2021; J. Jiang et al. 2023; P. X Luo & B. L. Tan 2024 etc.). Since the start of SC 25 from 2019 August 11, it has gone through more than 5.31 yr (up to 2024 November 30) and has actually entered its peak phase. So far, the strongest flare was an X9.0 flare that occurred on 2024 October 3, and no S-flare has occurred yet. We cannot help but ask: Will there be an S-flare in SC 25? How many S-flares will occur? When will they occur? Will there be more powerful flares during SC 25? These questions are very interesting and important, and they have received widespread attention and are extremely challenging for us (C. J. Schrijver 2007; D. S. Bloomfield et al. 2012; A. I. Khlystov 2014; L. A. Upton & D. H. Hathaway 2023).

Solar observations have become increasingly complicated: expensive multiple instruments, multiple frequency bands, high resolutions, big data, and various large-scale and complicated analysis techniques. However, we are still unable to effectively predict solar eruptions. S-flares and the more powerful flares should be the most spectacular large-scale explosions on the Sun. They should likely to respond to the simplest solar activity parameters, such as the DSN. If we could find some relatively simple indicator from the DSN records of the past four SCs to predict the occurrence of S-flares or even more powerful flares in the upcoming SC in advance, it would be greatly helpful, valuable, and operable. Section 2 introduces the main data used in this study, as well as the definition and extraction methods of relevant parameters. Section 3 presents the main results, linear regression functions, predicting results for SC 25, and the

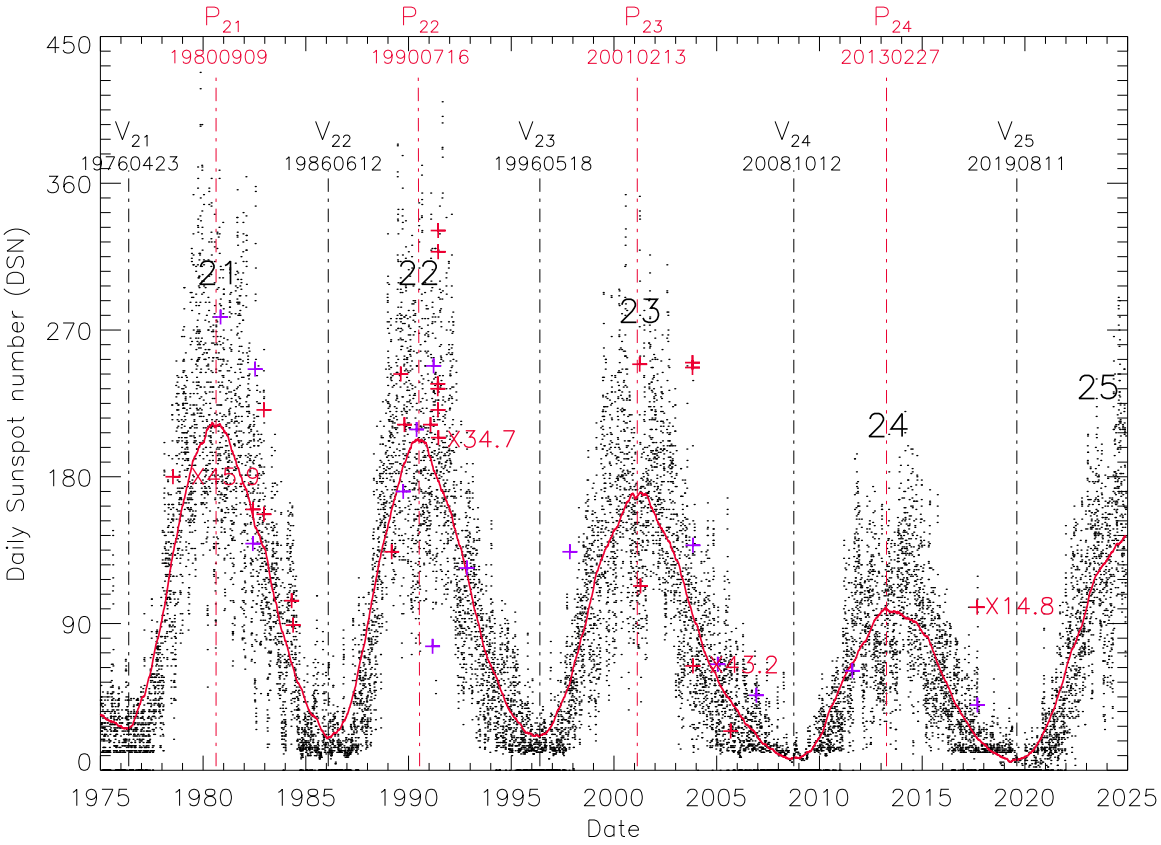

Figure 1. The distribution of the very large flares stronger than X10 (S-flare) during SC 21–25. The black dots are the DSNs with a smoothed curve (red). The purple pluses (+) mark the S-flares with the class of X10–X14.3 and the red pluses (+) mark the ES-flares (>*X*14.3). The vertical black and red dashed–dotted lines mark the valley and peak points of each cycle, respectively. Here, we also highlight the strongest flares for each SC.

possible physical explanation. The conclusions are summarized in Section 4.

2. Data and Parameter Extraction

2.1. Data Source

Here, we selected two kinds of long-term recorded observational data for our study:

(1) The relative DSN. This is one of the global indices of solar magnetic activities. The DSN data come from the World Data Center SILSO, which has adopted an open data policy; the data are corrected and assembled by standard methods (F. Clette & L. Lefevre 2016) and can be freely downloaded from the network (WDC-SILSO, Royal Observatory of Belgium, Brussels; website: https://www.sidc.be/index.php/SILSO/datafiles). Here, we directly obtain DSN records since 1818 January 1. Detailed information about the various diagnostics and corrections of DSN data can be found in K. J. Li et al. (2002) and F. Clette et al. (2014).

(2) The flare list observed at SXR wavelengths by GOES satellites. This is obtained from the GOES/SXR observation at the 1.0–8.0 and 0.5–4.0 Å wavelengths since 1975. GOES is a series of satellites, including GOES-1 to GOES-15 satellites from 1975 to 2017 and GOES-R series satellites since 2017, including the current GOES-16, GOES-17, and GOES-18 at present and GOES-19 in the future. GOES SXR observations provide a list of flares, including the location of the flaring active region on the solar disk. H. S. Hudson et al. (2024) found that SXR flares recorded by the old GOES series (GOES-1 to GOES-15) should be multiplied by a correction factor of 1.43 to be consistent with the GOES-R series (GOES-16 to GOES-19). Additionally, saturation also should be corrected for the strong flares (X-class and beyond). For example, after correcting the saturation, the previous listed X15 flare on 1978 July 11 is now X45.9, which is the strongest flare since 1975. The original X9.3 flare on 2017 September 6 is actually classified X14.8, which now becomes an S-flare. Totally, there are 37 S-flares during 1975–2024, which are marked in Figure 1 and listed in Table 1.

Figure 1 presents the distribution of S-flares on the profile of DSN from 1975 to 2024. There is an overlapped smoothed curve (red) of the DSN, which is designed to show clearly the valley and peak times of each cycle. The width of the smoothed window is chosen to ensure that each cycle has exactly a single valley and single peak. The purpose of doing this is to accurately pinpoint the start, peak, and end times of each cycle and to facilitate the phase of the cycle. Here, we obtained five valley points marked as V21, V22, V23, V24, and V25 (the black dotted–dashed vertical lines). They show the starts of SCs 21, 22, 23, 24, and 25, and also show the end of SCs 20, 21, 22, 23, and 24. The four red dotted–dashed vertical lines show the peak points of SCs 21, 22, 23, and 24, respectively. The pluses (+) mark the S-flares.

Figure 1 shows that S-flares do not directly respond to the very high DSN, and some S-flares occurred even with a very small DSN. A similar conclusion for X-class flares was reached

Table 1
List of the Solar S-class Flares during 1976–2024

No.	Date	DSN	Class	AR	S_{AR}	Location	t (yr)
1	19780711	180	X45.9	1203	1370	N20E46	2.22
2	19801106	278	X12.8	2776	1440	S12E74	4.54
3	19820603	139	X12.8	3763	1250	S09E72	6.11
4	19820606	160	X14.7	3763	1250	S09E25	6.12
5	19820712	246	X10.1	3804	2870	N11E37	6.22
6	19821215	221	X19.0	4026	640	S10E24	6.64
7	19821217	157	X14.7	4025	⋯	S08W21	6.65
8	19840424	104	X19.7	4474	2590	S12E43	8.00
9	19840520	89	X14.8	4492	670	S09E52	8.07
10	19890306	134	X19.3	5395	3570	N35E69	3.14
11	19890816	243	X28.0	5629	1320	S18W84	3.58
12	19890929	171	X14.2	5698	1250	S20W90	3.70
13	19891019	212	X23.1	5747	1160	S27E10	3.76
14	19900524	209	X14.1	6063	940	N33W78	4.35
15	19910125	212	X15.7	6471	2210	S16E78	5.03
16	19910304	76	X10.4	6538	⋯	S20E88	5.13
17	19910322	248	X13.8	6555	2530	S26E28	5.18
18	19910601	234	X28.3	6659	2300	N25E90	5.38
19	19910604	237	X32.0	6659	2300	N30E70	5.38
20	19910606	221	X30.2	6659	2300	N33E44	5.39
21	19910609	318	X15.1	6659	2300	N34E04	5.40
22	19910611	331	X17.0	6659	2300	N31W17	5.40
23	19910615	204	X34.7	6659	2300	N33W69	5.41
24	19921102	124	X13.3	7321	1650	S26W87	6.80
25	19971106	134	X13.1	8100	1000	S18W63	1.47
26	20010402	249	X29.6	9393	2440	N19W72	4.87
27	20010415	113	X21.1	9415	880	S20W85	4.91
28	20031028	247	X25.7	10486	2610	S16E08	7.44
29	20031029	250	X15.5	10486	2610	S15W02	7.45
30	20031102	138	X13.3	10486	2610	S14W56	7.46
31	20031104	64	X43.2	10486	2610	S19W83	7.46
32	20050120	65	X10.2	10720	1630	N14W61	8.68
33	20050907	24	X24.6	10808	1430	S11E77	9.30
34	20061205	46	X13.1	10930	680	S07E68	10.55
35	20110809	61	X10.7	11263	1320	N17W69	2.82
36	20170906	100	X14.8	12673	2060	S08W33	8.90
37	20170910	40	X13.0	12673	2060	S08W88	8.91

Note. AR: the NOAA number of S-flare active region, S_{AR}: the maximum area of the S-flare active region with unit of 10^{-6} solar hemisphere (μH), t: the occurring time after the start of the SC.

by H. S. Hudson (2007). Therefore, we cannot simply use the DSN to predict an upcoming S-flare.

2.2. Parameter Definitions

Our question about S-flares can be reflected in the following three parameters:

(1) How many S-flares occurred in an SC? N_s.
(2) When does the first S-flare occur during an SC? t_{s1}, which is defined as the time difference between the start of a cycle and the occurrence of the first S-flare.
(3) The mean time of all S-flares in an SC, t_{sm}. The time of an S-flare t is defined as the time difference between the start of the cycle and the onset of the S-flare. t_{sm} is defined as the time average of all S-flares that occurred in a cycle.

B. L. Tan (2019) reported that the mean DSN of valley phase was correlated with the magnitude of the forthcoming cycle. Therefore, it is possible to apply the parameters of valley phase

Table 2
The Characteristics of the DSN, X-class Flares (>X1.0), S-flares (>X10.0), ES-flares (>X14.3), and the Strongest Flare in Each SC

Parameter	SC 21	SC 22	SC 23	SC 24	SC 25
P_c	10.13	9.93	12.40	10.83	⋯
L_a	4.38	4.09	4.74	4.38	⋯
L_d	5.75	5.84	7.66	6.45	⋯
M_{sn}	428	410	353	220	⩾290
P_m	214.1	192.2	152.1	84.7	⋯
P_d	61.8	64.4	51.0	33.8	⋯
V_m	16.8	14.6	10.6	2.5	3.4
V_d	15.3	17.6	11.3	5.1	7.1
N_x	243	205	167	71	(108 ± 5)
t_{x1}	0.02	1.56	0.14	1.34	1.89
t_{xm}	4.75	4.00	6.05	5.12	⋯
N_s	9	15	10	3	(5 ± 2)
t_{s1}	2.22	3.14	1.47	2.82	⋯
t_{sm}	6.06	4.87	6.96	6.88	⋯
N_{es}	6	10	6	1	(2 ± 1)
t_{es1}	2.22	3.14	4.87	8.90	(7.46 ± 1.13)
t_{esm}	6.28	4.79	6.91	8.90	(8.31 ± 0.41)
t_{stg}	2.22	5.41	7.46	8.90	(8.78 ± 1.12)

Note. Here, the magnitudes of all flares that occurred before 2017 are corrected by the new calibration of H. S. Hudson et al. (2024) with a factor of 1.43. t_{x1}, N_x, and t_{xm} are the time of the first X-class flare, the number, and the mean time of X-class flares in an SC, respectively. t_{es1}, N_{es}, and t_{esm} are the time of the first ES-flare, the number, and the mean time of ES-flares in a cycle, respectively. t_{stg} is the time of the strongest flare in an SC. The values in parentheses represent the predicted values for SC 25 obtained in this work.

to predict the occurrence of S-flares in advance before the start of cycles. Here, we define the following parameters to describe the valley phase of an SC:

(1) The mean DSN during the valley phase, V_m, which reflects the valley level before the start of a cycle.
(2) The rms deviation of the DSN during the valley phase, V_d, which reflects the degree of variation of the DSN around the valley phase.

In order to study the corresponding physical mechanism, we also extracted the following parameters to describe the cycle:

(1) Period of the SC, P_c, defined as the time interval between the start and end of a cycle.
(2) Length of the ascending phase of the SC, L_a, defined as the time interval between the start and peak of a cycle.
(3) Length of the descending phase of the SC, L_d, defined as the time interval between the peak and end of a cycle. Obviously, we have $P_c = L_a + L_d$.
(4) The maximum DSN of an SC, M_{sn}.
(5) The mean DSN during the peak phase, P_m, which reflects the solar activity level of a cycle.
(6) The rms deviation of the DSN during the peak phase, P_d, which reflects the degree of variation of the DSN around the peak phase.

All above parameters for SCs 21–24 can be extracted from Figure 1 and listed in Table 2. The width of the valley or peak phases is defined as a period during which the DSN changes relatively flat before and after the valley or peak points. Here we hope to remove the influence of the last descending phase and the next ascending phase. Based on careful comparisons, we found that when the half width of the valley or peak phase

was set as 150 days (totaly 300 days), the data were relatively flat; beyond this width, the trend of the data changes in an arc, which may contain influence of the last ascending phase or the next descending phase.

3. Results, Predictions, and the Related Mechanism

3.1. The Correlations Between the Occurrence of S-flares and the Parameters of SCs

Figure 1 shows that S-flares do not strongly depend on the DSN. In SC 23, the strongest flare (X43.2 on 2003 November 4) corresponds to a DSN of 64, while the maximum DSNs of this cycle are high up to 353. In fact, when the DSN reaches the maximum of an SC, there is always no powerful flare that has occurred. For example, the DSN reached a maximum of SC 24 on 2014 February 27, but that day only produced 12 C-class flares and no more powerful flares. The other cycles also have a similar trend. These facts indicate that there is no obvious correlation between the DSN and the occurrence of S-flares. It is difficult to predict the occurrence of S-flares simply from the DSN.

Table 1 lists the parameters of 37 S-flares, including their date, the corresponding DSN and active region, its maximum area and position on the solar disk, and the time of the occurrence after the start of the corresponding SC.

Based on carefully scrutinizing the distribution of S-flares, we find that they can be classified into two types: isolated S-flare and S-flare groups.

(1) Isolated S-flare refers to only one S-flare generated from an active region. For example, active region NOAA 10808 only generated an X24.6 class flare on 2005 September 6 and no other S-flare. Among the 37 S-flares listed in Table 1, there are 23 isolated S-flares (62%).
(2) S-flare group refers to at least two or more S-flares generated from an active region, which can be regarded as a group of homologous flares. The most famous S-flare group occurred from 2003 October 28 to November 4 in active region NOAA 10486 with four S-flares (X25.7, X15.5, X13.3, and X43.2). The most spectacular S-flare group occurred from 1991 June 1 to 15 in active region NOAA 6659 with six S-flares (from X15.1 to X34.7).

From Figure 1 and Table 1, we may get the following conclusions:

(1) Each SC has only one S-flare group active region, which is NOAA 3763 in SC 21 (two S-flares), NOAA 6659 in SC 22 (six S-flares), NOAA 10486 in SC 23 (four S-flares), and NOAA 12673 in SC 24 (two S-flares). All S-flare groups occurred in the descending phase of solar cycles.
(2) Most S-flares tend to occur after the peaks of SCs, $t_{sm} > L_a$. This result confirms an earlier conclusion that the more powerful flares tends to occur later in the SC (B. L. Tan 2011). Among the 37 S-flares, there are 29 (about 78.4%) that occurred in the descending phases of SCs, and only 8 (21.6%) S-flares occurred in the ascending phase. Additionally, except for SC 22, in which most S-flares occurred near the peak phase, almost all other S-flares occurred in the descending phase, even far away from the peak point. For example, in SC 21, only 1 S-flare occurred in the ascending phase (X45.9, on 1978 July 11), while all other 8 S-flares occurred in the descending phase, and the last S-flares even occurred on 1984 May 20, 8.07 yr after the start of the cycle. In SC 23, the last S-flare even occurred on 2006 December 5, 10.55 yr after the start of the cycle.
(3) Most S-flares tend to occur in low-latitude regions on the Sun. Among the 37 S-flares, 26 (70%) occurred in low-latitude regions with latitude $\leqslant 20°$, while the other 11 S-flares (30%) occurred in high-latitude regions with latitudes $>25°$. As for the S-flare active regions, 23 of them (85%) occurred in low-latitude regions, and only 4 (15%) occurred in high-latitude regions. Additionally, all the high-latitude S-flares occurred in SC 22 (from 1989 March to 1991 June).
(4) The occurrence time of the strongest flare (t_{stg}) in each SC is strongly anticorrelated with the intensity of the cycle (M_{sn}, P_m, and V_m). The stronger the SC, the earlier the strongest flare occurred, while the weaker the cycle, the later the strongest flare occurred.

Table 2 lists all parameters of S-flares (N_s, t_{s1}, and t_{sm}) and SCs (P_c, L_a, L_d, M_{sn}, P_m, P_d, V_m, and V_d) during SCs 21–25. In order to compare different class of flares, we also listed the parameters of X-class flares (>X1.0), the extremely strong flares (>X14.3, ES-flares), and the strongest flare in each SC. Here, totally there are 719 X-class flares, 37 S-flares, and 23 ES-flares during SCs 21–24. The magnitudes of all flares occurred before 2017 are corrected by the new calibration of H. S. Hudson et al. (2024) with a factor of 1.43.

Table 3 presents the correlation coefficients (Cr) between the parameters of X-class flares, S-flares, ES-flares, and the parameters of SCs.

Table 3 shows that the time of the first S-flare (t_{s1}) and the mean time of all S-flares (t_{sm}) in each SC are not correlated with the mean DSN (V_m) and rms deviation of the DSN (V_d) in the cycle's valley phase. A similar regime also occurs in X-class flares. These facts indicate that the occurrence of S-flares as well as X-class flares has a clear randomness, and it is difficult to use the parameters of the SC to predict their occurrence in advance. Then, what about more powerful flares, the ES-flares?

Here, we choose to define a flare exceeding X14.3 (equal to $>X10$ in the old GOES SXR level before Hudson's recalibration) as an extremely strong flare (ES-flare). Totally, there are 23 ES-flares since 1975, and SC 24 has only 1 ES-flare, which is rare enough and extremely strong. Table 3 presents the values of Cr between the parameters of ES-flares and SCs. We find:

(1) Similar to S-flares, most ES-flares tend to occur after the peak of cycles. Among the 23 ES-flares, 19 (82.6%) occurred in the descending phases, and only 4 (17.4%) S-flares occurred in the ascending phase.
(2) Also similar to S-flares, most ES-flares tend to occur in low-latitude regions on the Sun. Among the 23 ES-flares, 15 (65%) occurred in low-latitude regions with latitude $\leqslant 20°$, while the other 8 ES-flares (35%) occurred in high-latitude regions with latitudes $>25°$. As for the ES-flare active regions (ESARs), 13 of them (81%) distributed in low-latitude regions and only 3 (19%) distributed in high-latitude regions.
(3) Different from S-flares and X-class flares, there are strong correlations between the occurrence of ES-flares and the parameters of SCs. N_{es} is strongly correlated with V_d

Table 3
The Correlation Coefficients (Cr) between Parameters of X-class Flares (>X1.0), S-flares (>X10.0), ES-flares (>X14.3), the Strongest Flare, and Parameters of SCs 21–24

Parameter	t_{x1}	t_{xm}	N_x	t_{s1}	t_{sm}	N_s	t_{es1}	t_{esm}	N_{es}	t_{stg}
P_c	−0.44	0.95	−0.37	−0.81	0.76	−0.23	0.34	0.41	−0.29	0.56
L_a	−0.72	0.98	−0.23	−0.94	0.85	−0.36	0.22	0.45	−0.39	0.30
L_d	−0.32	0.91	−0.41	−0.75	0.71	−0.19	0.37	0.38	−0.25	0.62
*M*sn	−0.39	−0.38	0.99	−0.13	−0.64	0.82	−1.00	0.90	0.86	−1.00
P_m	−0.39	−0.43	1.00	−0.08	−0.65	0.76	−1.00	0.87	0.81	−1.00
P_d	−0.22	−0.51	0.97	0.02	−0.76	0.89	−0.98	−0.96	0.92	−0.82
V_m	−0.40	−0.40	1.00	−0.11	−0.64	0.77	**−1.00**	−0.87	0.82	**−1.00**
V_d	−0.12	−0.57	0.94	0.11	−0.82	0.91	**−0.95**	**−0.98**	**0.95**	−0.77

(Cr = 0.95). t_{es1} is strongly anticorrelated with V_d (Cr = −0.95) and V_m (Cr = −1.00). t_{esm} is strongly anticorrelated with V_d (Cr = −0.98). Since the accurate values of V_d and V_m can be obtained before the start of the SC, it is possible to apply the above strong correlations to predict the occurrence of ES-flares in advance. This fact hints at an essential difference between X-class flares <X14.3 and ES flares >X14.3.

3.2. Regression, Fitting Functions, and Predictions

3.2.1. The Number of ES-flares in an SC

The strong correlation between N_{es} and V_d indicates that we may predict N_{es} for the upcoming SC. As N_{es} is an integer rather than real-valued variable, here we apply the Poisson regression (A. C. Cameron & P. K. Trivedi 1998; J. S. Long & J. Freese 2006) to show quantitatively the dependence of N_{es} on V_d and V_m. Figure 2 presents the results of Poisson regression, which predicts that SC 25 possibly will have 2 ± 1 (or say: 1 ~ 3) ES-flares. Here, the prediction of the regression between N_{es} and V_d output is 2.3 ± 1.1, while the prediction of the regression between N_{es} and V_m output is 2.2 ± 1.2. Both results are close to each other, but the former has higher credibility, for its pseudo-R-squ. is higher (0.8372) than the latter (0.7466). The left panel of Figure 2 shows that the observational results distributed approximately along the diagonal, while right panel shows that the results distributed more dispersedly from the diagonal.

Because of the high correlation coefficient between N_{es} and V_d (Cr = 0.95), as a comparison, we also apply a linear regression to show a heuristic fitting function (overplotted with the green thick dashed–dotted line in the left panel of Figure 2), $N_{es} \approx -2.16 + 0.63V_d \pm 1.05$. As for SC 25, $V_d = 7.1$ and $V_m = 3.4$. Substituting these values into the above expression, then $N_{es} \approx 2.31 \pm 1.05$, which is also close to the result derived from the above Poisson regression, or simply to say, SC 25 will have 1 ~ 3 ES-flares. Using the same method and the strong correlations between N_x and V_m (Cr = 1.00) and between N_s and V_d (Cr = 0.91), we derived that SC 25 will have 108 ± 5 X-class flares and 5 ± 2 S-flares.

The above results imply that the number of ES-flares in the upcoming SC is strongly depending on V_d. The higher the V_d, the more the ES-flares occurring in that cycle. The left panel of Figure 2 showed that the distributions of SCs 21–24 are approximately concentrated near the diagonal.

3.2.2. The Occurrence Time of ES-flares

Then, when will these ES-flares occur? Let us first examine the mean time of occurrence of ES-flares (t_{esm}) in each cycle.

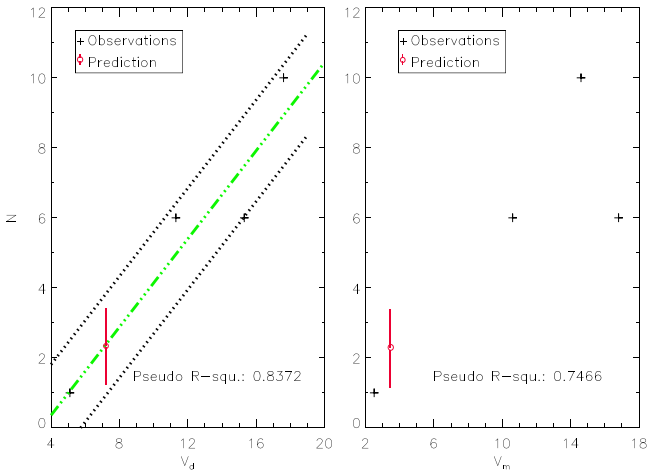

Figure 2. The results of Poisson regression of the number of ES-flares (N_{es}) in SC vs. the rms deviation of the DSN (V_d, left) and mean DSN (V_m, right) around the cycle valley. The green thick dashed–dotted line is a heuristic fitting function obtained from linear regression, while the red circle is the predicting results for SC 25 in this work.

Table 2 shows that the strongest correlation takes place between t_{esm} and V_d with Cr = −0.98. The red triangles of the left panel of Figure 3 plot the distribution that concentrated approximately along the opposite diagonal. From the linear regression, we may obtain a best-fitting function:

$$t_{esm} \approx 10.48 - 0.31V_d \pm 0.30. \quad (1)$$

Substituting the value of V_d for SC 25, we obtain $t_{esm} \approx 8.31 \pm 0.30$ yr. This implies that the possible 2 ± 1 ES-flares in SC 25 will take place averagely 8.31 yr after the valley point (2019 August 11).

Now, we try to answer another question: when will the first ES-flare occur in an SC? Table 2 shows that the correlation coefficient between t_{es1} and V_m is high up to −1.00, a very strong anticorrelation, and the related distribution is shown in the right panel of Figure 3 (black part). The linear regression derived a best-fitting function:

$$t_{es1} \approx 9.33 - 0.47V_m \pm 0.69. \quad (2)$$

With this function, we may get a prediction for SC 25: $t_{es1} \approx 7.73 \pm 0.69$ yr. That is to say, the first ES-flare will occur around 2027 May. At the same time, the correlation coefficient between t_{es1} and V_d is −0.95, also a strong anticorrelation, and the related distribution is shown in the left panel of Figure 3 (black), and the linear regression function can be obtained as

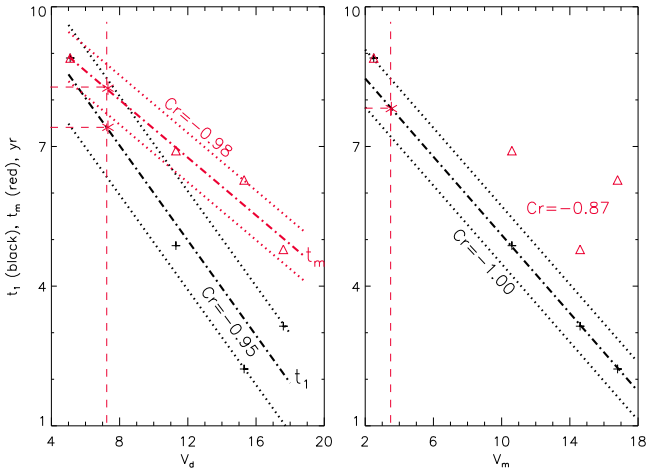

Figure 3. The occurring time of ES-flares in SCs vs. the rms deviation of the DSN (V_d, left) and mean DSN (V_m, right) during the cycle valley. The black parts (including +, the fitted thick dashed–dotted lines, and thin dotted lines) show the time of the first ES-flare in SCs t_{es1}, while the red parts show the mean time of all ES-flares in SC, t_{esm}. The red $*$ is the predicting results for SC 25 in this work.

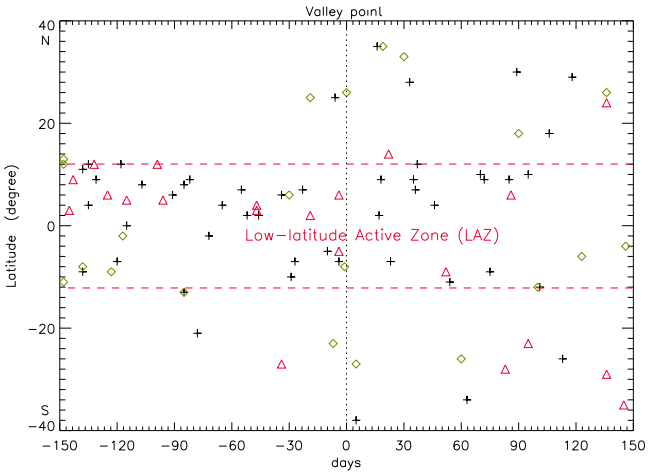

Figure 4. The latitude distribution of sunspot active regions that occurred during valley phases of SCs 23 (black +, from 1995 December 20 to 1996 October 15), 24 (green ◊, from 2008 May 14 to 2009 March 11), and 25 (red △, from 2019 March 14 to 2020 January 8). The 0 point on the x-axis represents the valley point between the two SCs. The area between two red dashed lines represents the LAZ.

follows:

$$t_{es1} \approx 11.10 - 0.51V_d \pm 0.80. \quad (3)$$

Substituting $V_d = 7.10$ into the above expression, we get $t_{es1} = 7.48 \pm 0.80$ yr, which is in about 2027 January or February. Additionally, we may attempt to apply binary linear regression to obtain a best-fitting function of t_{es1} with respect to V_d and V_m:

$$t_{es1} \approx 9.45 - 0.46V_m - 0.0125V_d \pm 0.62. \quad (4)$$

It derived $t_{es1} \approx 7.80 \pm 0.62$ yr (around 2027 May or June). Obviously, the above three predicting results ($t_{es1} = 7.73 \pm 0.69$, 7.48 ± 0.80, and 7.80 ± 0.62 yr) are essentially very close to each other. In order to ensure a more reliable prediction, we list the predicted value of 7.48 ± 0.80 for SC 25 in Table 2. In brief, SC 25 will possibly have about 1–3 ES-flares, and all of them will occur after the spring of 2027.

3.2.3. The Occurrence Time of the Strongest Flare

Using the strong anticorrelation between t_{stg} and V_m ($Cr = -1.00$), we may obtain the linear regression function:

$$t_{stg} \approx 10.11 - 0.393V_m \pm 0.93. \quad (5)$$

It derived that the occurrence time of the strongest flare in SC 25 is about $t_{stg} \approx 8.78 \pm 0.93$ yr (around 2028 May).

Here, it is necessary to emphasize that the above results are only based on a small data set with four SCs since 1975, which should contain significant uncertainty. Strictly speaking, it is difficult to obtain exact statistical results with such a small data set. Therefore, we chose the parameter pairs with high correlation coefficient $\geqslant 0.95$ for a heuristic prediction, and the corresponding confidence level exceeds 95%. Table 3 listed that there are three other pairs of parameters between t_{es1} and M_{sn}, P_m, and P_d during the peak phase that are anticorrelated with coefficients of Cr exceeding 0.95. Because M_{sn}, P_m, and P_d actually reflect the intensity of the SC, these anticorrelations imply that the stronger the SC, the earlier ES-flares occur. However, due to most ES-flares occurring after the peak phase or even in the descending phase of SCs, the application of predicting ES-flares has little practical significance. On the contrary, the valley parameters of SCs are generally at least 2 yr earlier than the first ES-flares (last column in Table 1), and they can serve as precursors for predicting ES-flares, which has practical operability.

3.3. Physical Explanations

Why do most of the S-flares and ES-flares occur in the late phase of SCs and low-latitude regions on the solar disk? Why is the occurrence of S-flares in the SC somewhat accidental, while the occurrence of ES-flares is significantly correlated with the DSN during the valley phase of SCs?

Generally, large active regions should have more complex magnetic field structures and are more prone to producing strong flares (I. Sammis et al. 2000), such as the superactive region (SAR) with $\beta\gamma\delta$-type magnetic configuration (T. Bai 1987; L. R. Tian et al. 2002; A. Q. Chen et al. 2011). Table 1 lists the NOAA number, maximum area, and location of ESARs, which shows that the 23 ES-flares originated from 16 ESARs, of which 12 have a maximum area exceeding 1000 μH and should be SARs. At the same time, we also noted that many very large $\beta\gamma\delta$-type complex SARs had no S-flare or ES-flare, such as NOAA 3776 (3100 μH), 5669 (3080 μH), and 12192 (2710 μH), etc. These facts indicate that SARs are not the essential condition for generating ES-flares. The generation of ES-flares should be related to the early evolution of SCs, such as V_m and V_d.

Let us look at the latitude distribution of valley sunspot regions (VSRs). Figure 4 presents their latitude distributions in SCs 23, 24, and 25. Most of them are simple α- or β-type active regions, with an area of less than 150 μH and lifetime of 2–10 days. There are about 75% of VSRs distributing in a zone within 12° north and south latitude of the Sun, while the other 25% of VARs are distributed in high latitudes beyond 12° to about 40°. This fact indicates that even during the valley phases of SCs, although the sunspot number is very small, magnetic activity still exists in the low-latitude region. It hints that the low-latitude region may be a long-term active zone possibly different from the new emerging sunspot region in the upcoming SC, called the low-latitude active zone (LAZ), which always keeps a certain level of activity during the valley phase of the SC. Solar dynamo theory has indicated that the toroidal magnetic field is generated from a poloidal field due

to the solar differential rotation. In each SC, the new emerging sunspot region first appeared in high-latitude regions (near 40°) and then gradually migrated to low-latitude regions and finally arrived at about 5°–8° latitude near the end of the cycle (H. W. Babcock 1961; R. B. Leighton 1969). Due to the enormous energy accumulation required for ESAR to generate ES-flares, it is not easy to provide such conditions in a typical active region. Considering that most ES-flares occurred in regions with latitudes below 20° and in the late phase of SC, we suggest that ES-flares should be mainly generated from the interaction between the newly emerging active region and LAZ. Such interaction may lead to large-scale energy accumulation and most powerful eruption. In the early phase (such as the ascending phase) of SCs, the newly emerging active regions located in high latitude and far from LAZ, their interaction should be very weak and difficult to produce ES-flares. On the contrary, in the late phase (such as the descending phase) of SCs, the newly emerging active regions occurred at low latitude and very close to the LAZ, so their interaction should become very strong and tend to produce extremely powerful ES-flares. The values of V_d and V_m are mainly dominated by the sunspots in the LAZ during the valley phase before the onset of SCs. B. L. Tan (2019) reported that the strength of an SC is related to the mean DSN during the valley phase. Tables 2 and 3 also show that, besides being strongly anticorrelated with V_d and V_m, t_{es1} is also strongly anticorrelated with M_{sn}, P_m, and P_d. This actually indicates that the stronger the SC, the more the ES-flares and the earlier the ES-flares occurred.

As mentioned in Section 3.1 and Table 1, there are 8 ES-flares that occurred in high-latitude regions beyond 25°. All of them generated from 3 ESARs (NOAA 5395, 5747, and 6659) around the peak phase of SC 22 (from 1989 March to 1991 June). Especially, the active region NOAA 6659 produced 6 ES-flares, demonstrating the uniqueness of this SC. This fact indicates that in addition to the interaction between LAZ and the newly emerging active regions, other mechanisms may also contribute to generate ES-flares, such as interactions between the nearby active regions (collisions, mergers, and magnetic induction, etc.) or the evolution of large active regions themselves. Among the 23 ES-flares, 8 come from high-latitude regions, accounting for 35%, and among the 16 ESARs, there are 3 high-latitude ESARs, accounting for 19%. This indicates that the interaction between LAZ and the newly emerging active regions should be the main mechanism for the formation of ES-flares.

4. Summary and Discussion

Based on the analysis of the DSNs and GOES SXR observations since 1975, we obtained the following conclusions regarding S-flares:

(1) Both S-flares and the stronger ES-flares mostly occur in the late phases of SCs and low-latitude regions on the solar disk.

(2) Similar to X-class flares, the occurrence of S-flares (>X10) in each SC is somewhat random, but ES-flares (>X14.3) seem to be dominated by V_m and V_d. The number of ES-flares in a cycle is strongly correlated with V_d, and the time of the first ES-flare is strongly anticorrelated with V_m and V_d. The mean time of all ES-flares in a cycle is strongly anticorrelated with V_d (Figures 2 and 3). The stronger the SC, the earlier the strongest flare occurs.

(3) V_d and V_m can be applied to predict the number and timing of ES-flares in the forthcoming SCs. The linear regressions may derive some heuristic fitting functions of N_{es} versus V_d, t_{es1} versus V_m, t_{es1} versus V_d, t_{esm} versus V_d, and t_{stg} versus V_m. Based on these strong correlations and regression fitting functions, we may predict the ES-flares in SC 25: about 2 ± 1 ES-flares, and the first ES-flare may occur around the spring of 2027, which is slightly close to the end of the cycle. This result indicates that for space weather forecasting, 2027 possibly should be a key year and require special attention.

Here, it should be emphasized that the above conclusions are based on a small data set of the past four SCs, and thus they are only heuristic and require further verification with more observations in the future.

Further analysis shows that the occurrence of ES-flares during an SC is closely related to the cycle intensity: the stronger the SC, the higher the V_m and V_d, and the more ES-flares there are, and the earlier they occur. We proposed that the Sun may have an LAZ, and most ES-flares are the results of the interaction between the newly emerging active regions and LAZ. In the early phase of SC, the newly emerging active region is located in the high-latitude region, far away from the LAZ, with weak interaction, making it less likely to produce ES-flares. On the contrary, in the late phase of the SC, the newly emerging active region is located in the low-latitude region, close to the LAZ, with strong interaction and easy-to-generate ES-flares. This explains why most of the ES-flares occurred in the late phase of SCs and near the low-latitude regions on the solar disk.

Here, we are also soberly aware that the LAZ is only a preliminary assumption just derived from limited observations, and it requires more observation and theoretical research to confirm. In fact, LAZ is somewhat similar to the equatorial low-pressure zone formed by the compression of trade winds from the northern and southern hemispheres of Earth, mainly due to the rotation of the celestial body. In the near future, we will continue to delve into the characteristics and evolutions of the solar LAZ and the generations of ES-flares in order to provide a more reliable physical basis for understanding the generation of ES-flares, predicting their occurrence and the possible disastrous space weather events.

Acknowledgments

This work is supported by the Strategic Priority Research Program of the Chinese Academy of Sciences XDB0560000, the National Key R&D Program of China 2021YFA1600503, 2022YFF0503001, and the International Partnership Program of Chinese Academy of Sciences 183311KYSB20200003.

ORCID iDs

Baolin Tan https://orcid.org/0000-0003-2047-9664
Jing Huang https://orcid.org/0000-0001-8250-1535
Kaifan Ji https://orcid.org/0000-0001-8950-3875

References

Babcock, H. W. 1961, ApJ, 133, 572
Bai, T. 1987, ApJ, 314, 795
Bai, T., & Sturrock, P.A. 1989, ARA&A, 27, 421
Bloomfield, D. S., Higgins, P. A., McAteer, R. T. J., & Gallagher, P. T. 2012, ApJL, 747, L41

Cameron, A. C., & Trivedi, P. K. 1998, Regression Analysis of Count Data (Cambridge: Cambridge Univ. Press)
Chen, A. Q., Wang, J. X., Li, J. W., Feynman, J., & Zhang, J. 2011, A&A, 534, A47
Clette, F., Leif, S., Jose, M. V., & Edward, W. C. 2014, SSRv, 186, 35
Clette, F., & Lefevre, L. 2016, SoPh, 291, 2629
Cliver, E. W., Schrijver, C. J., Shibata, K., & Usoskin, I. G. 2022, LRSP, 19, 2
Emslie, A. G., Dennis, B. R., Shih, A. Y., et al. 2012, ApJ, 759, 71
Guo, W., Jiang, J., & Wang, J. X. 2021, SoPh, 296, 136
Hayakawa, H., Bechet, S., Clette, F., et al. 2023, ApJ, 954, L3
Harrison, R. A. 1995, A&A, 304, 585
Hudson, H. S. 2007, ApJ, 663, L45
Hudson, H. S., Cliver, E., White, S., et al. 2024, SoPh, 299, 39
Jiang, J., Zhang, Z. B., & Petrovay, K. 2023, JASTP, 234, 106018
Khlystov, A. I. 2014, IzAOP, 50, 776
Leighton, R. B. 1969, ApJ, 156, 1
Li, K. J., Zhan, L. S., Wang, J. X., et al. 2002, A&A, 392, 301
Long, J. S., & Freese, J. 2006, Regression Models for Categorical Dependent Variables Using Stata (College Station, TX: Stata)
Luo, P. X., & Tan, B. L. 2024, RAA, 24, 035016
Maehara, H., Shibayama, T., Notsu, S., et al. 2012, Natur, 485, 478
Notsu, Y., Maehara, H., Honda, S., et al. 2019, ApJ, 876, 58
Pesnell, W. D., & Schatten, K. H. 2018, SoPh, 293, 112
Schrijver, C. J. 2007, ApJ, 655, L117
Sammis, I., Tang, F., & Zirin, H. 2000, ApJ, 540, 583
Schaefer, B. E., King, J. R., & Deliyannis, C. P. 2000, ApJ, 529, 1026
Shibayama, T., Maehara, H., Notsu, S., et al. 2013, ApJS, 209, 5
Tan, B. L. 2011, Ap&SS, 332, 65
Tan, B. L. 2019, AdSpR, 63, 617
Tian, L. R., Liu, Y., & Wang, J. X. 2002, SoPh, 209, 361
Upton, L. A., & Hathaway, D. H. 2023, JGRA, 128, e2023JA031681